Clickable amino acid tuned self-assembly of a nucleus-selective multi-component nanoplatform for synergistic cancer therapy†

Lan Yang,[a] Xiao He,[a] Zhiying Zeng,[a] Jiakun Tang,[a] Dongmei Qi,[a] Huijie Ma,[a] Hui Chen,*[a] Xinghai Ning [ID] *[b] and Xuli Feng [ID] *[a]

Nucleus-targeted therapy holds great promise in cancer treatment; however, a lack of effective nucleus-specific delivery significantly limits its application potential. Here, we report a nucleus-targeted synergistic chemo-photodynamic therapy based on the self-assembly of chlorin e6 (Ce6) and doxorubicin (DOX) tuned by clickable dibenzocyclooctyne (DIBO) functionalized lysine (D-K) and subsequent reaction with crosslinkers. The assembled nanodrugs with high loading efficiency and long-term stability show enhanced cellular uptake and accumulation in the nucleus, resulting in greatly improved *in vitro* and *in vivo* chemo-photodynamic efficacy. Notably, D-K can promote the rapid self-assembly of Ce6 and DOX in aqueous solution, avoiding the introduction of organic solvents or tedious preparations. In addition, the introduction of the DIBO group can effectively expand the types of self-assembly material and enhance the self-assembly behaviour through a copper-free click reaction. Therefore, we present an effective nucleus-targeted combination drug delivery strategy, which has great potential in the treatment of many diseases.

Introduction

Over the past decade, organelle-targeted therapy has been emerging as a promising anticancer approach. In comparison to other apoptosis-associated cellular components, such as mitochondria and lysosomes, the nucleus plays a critical role in most biological cellular processes, and exhibits high sensitivity to various types of DNA damage, making it a promising target for antitumor therapy. Chemotherapy is one of the most commonly used treatments for various cancers.[1,2] In recent years, chemotherapy has been combined with other treatment strategies such as photodynamic therapy (PDT) to overcome the limitations of traditional single treatments through different modes of action.[3–8] PDT has been recognized as a potent strategy for advanced combination treatment.[9–12] However, the inherent drawbacks of concurrent PDT, including low bioavailability and poor systemic circulation, are still major obstacles to its clinical applications.[13] To improve the PDT efficiency, various carriers have been developed, such as

liposomes, and polymeric and inorganic nanoparticles.[14–17] Unfortunately, most of these carriers suffer from technical problems of inconvenient preparation, low drug loading efficiency and poor stability.[18,19] In addition, the efficacy of PDT largely depends on the subcellular localization of photosensitizers (PS) due to the short transient lifetime and diffusion range of reactive oxygen species (ROS).[20] Thus, selective generation of ROS in specific organelles, such as the nucleus, that are more susceptible to oxidative damage may significantly improve therapeutic efficacy. Furthermore, the nucleus-targeting delivery strategy makes it efficient to transport DOX into the nucleus, which can induce direct inhibition of the DNA or RNA synthesis process, while avoiding the *P*-glycoprotein associated efflux pumping of DOX. Therefore, an effective strategy that directly transports PS and DOX into cancer cell nuclei is greatly needed for improving the combination treatment of PDT and chemotherapy.

Molecular self-assembly is a versatile process that involves an organized arrangement of molecules through non-covalent interactions.[21–23] Various biomolecules including proteins, peptides, and even amino acids have been employed as building blocks for the construction of functional nanomaterials.[24–28] In particular, amino acids and their derivatives (*e.g.*, fluorenylmethyloxycarbonyl (Fmoc) modified amino acids) offer appreciable advantages over proteins and peptides in the construction of nanoarchitectured functional systems, due to their molecular simplicity, biostability, and inherent biocompatibility.[29,30] Recent studies show that amino acids can

[a]*Chongqing Key Laboratory of Natural Product Synthesis and Drug Research, School of Pharmaceutical Sciences, Chongqing University, Chongqing 401331, China. E-mail: chenhui0429@cqu.edu.cn; fengxuli@cqu.edu.cn*

[b]*National Laboratory of Solid State Microstructures, Chemistry and Biomedicine Innovation Center, College of Engineering and Applied Sciences, Jiangsu Key Laboratory of Artificial Functional Materials, Nanjing University, Nanjing 210093, China. E-mail: xning@nju.edu.cn*

† Electronic supplementary information (ESI) available: Experimental details and supplementary figures. See DOI: 10.1039/d1sc01073e

spontaneously assemble to form ordered nanomaterials with various morphologies by simply manipulating the coordination and noncovalent interactions.[31–35] Although amino acid self-assembly exhibits benefits for integrating drugs into therapeutic nanoparticles,[36,37] no studies have actually managed to develop nucleus-targeted nanodrugs. To accomplish this task, there is an urgent need for a new amino acid self-assembly method to achieve selective delivery of therapeutics not only to the same cells, but also to therapeutically active sites in the nucleus.

Here, we present a sequential self-click-assembly strategy, which utilized amphiphilic amino acid **D-K** mediated self-assembly to construct multi-component nanoplatforms for nucleus-targeted delivery of PS and anticancer drugs. As shown in Scheme 1a, the traditional amino acid protecting group Fmoc was changed to the dibenzocyclooctyne (DIBO) functional group in **D-K** mainly for copper-free click chemistry, which can effectively expand the types of self-assembly material and enhance the self-assembly behaviour under mild conditions. Ce6 and DOX molecules can be integrated into the amphiphilic networks of **D-K** through multiple weak intermolecular interactions, including π–π stacking, hydrophobic and electrostatic interactions, and then assembled with azide crosslinkers (**4-A**) through a copper-free click reaction to generate a D-KCD/A multi-component nanoplatform. D-KCD/A could not only improve the drug loading efficacy, but also enhance the accumulation of Ce6 and DOX in the nucleus, which greatly enhanced the synergistic effects of *in vitro* and *in vivo* PDT and

chemotherapy (Scheme 1B). Thus, D-KCD/A represents a promising nucleus-targeted platform for combination therapy, and may have potential for improving the management of malignant diseases.
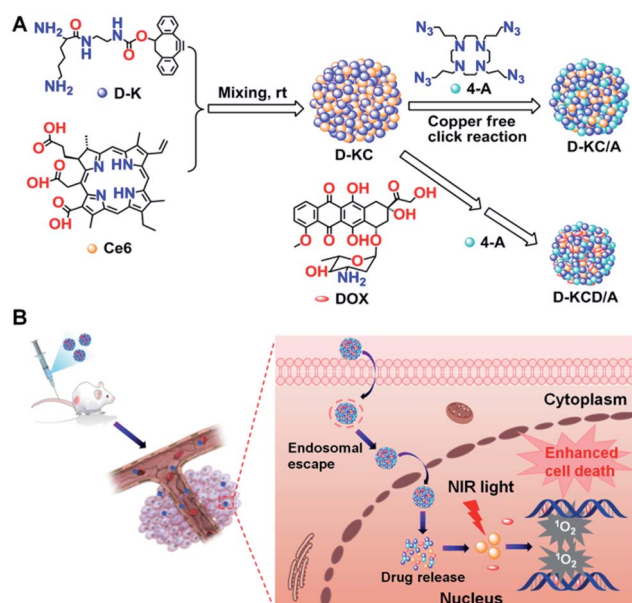
Results and discussion

Synthesis of D-K and 4-A

The synthesis of **D-K** and **4-A** is illustrated in Fig. 1. Initially, Boc-lysine-NHS was reacted with ethylenediamine to afford compound **1**, which was reacted with 4-nitrophenyl chloroformate-substituted DIBO to get compound **2**. The final **D-K** was obtained by deprotecting the Boc groups with hydrochloric acid. 3-Azido-1-propanol was reacted with triflic anhydride to get compound **3**, which was further reacted with tetraazacyclododecane to afford **4-A**. All intermediates and final compounds were carefully characterized and confirmed by nuclear magnetic resonance (NMR) and mass spectroscopy (MS).

Preparation and characterization of D-K tuned self-assembly

We next investigated the capability of **D-K** to regulate the self-assembly of nanoparticles loaded with Ce6 and DOX. The morphology and size of nanoparticles containing different components were identified using transmission electron microscopy (TEM) and dynamic light scattering (DLS). As shown in Fig. 2A and B, loose nanoparticle agglomerates (D-KC) were formed upon mixing **D-K** (0.233 mg mL^{-1}) and Ce6 (0.08 mg mL^{-1}), and had an average diameter of 250 nm and zeta potential of about 8 mV (Fig. 2C). However, D-KC was transformed into a compact nanostructure after crosslinking with **4-A** (0.067 mg mL^{-1}), generating D-KC/A with the decrease of particle sizes and the increase of zeta potentials. Importantly, we found that the integration of DOX (0.08 mg mL^{-1}) into D-KC/A had no effects on the morphology of the nanoparticles (D-KCD/A), but a smaller size and higher zeta potential were observed, indicating that DOX further enhances the hydrophobic and electrostatic interactions within nanoparticles. It is worth noting that the particle size of both D-KC/A and D-KCD/A measured by DLS was larger than that observed by TEM, which

Scheme 1 Schematic illustration of **D-K** tuned self-assembly of Ce6 and DOX for nucleus-targeted synergistic chemo-photodynamic therapy. (A) Schematic of the formation of D-KCD/A nanoparticles *via* **D-K** tuned self-assembly of Ce6 and DOX based on π–π stacking, hydrophobic and electrostatic interactions. (B) Schematic illustration of self-assembled D-KCD/A nanoparticles for nuclear accumulation of Ce6 and DOX to greatly improve the synergistic antitumor efficacy of chemo-photodynamic therapy.
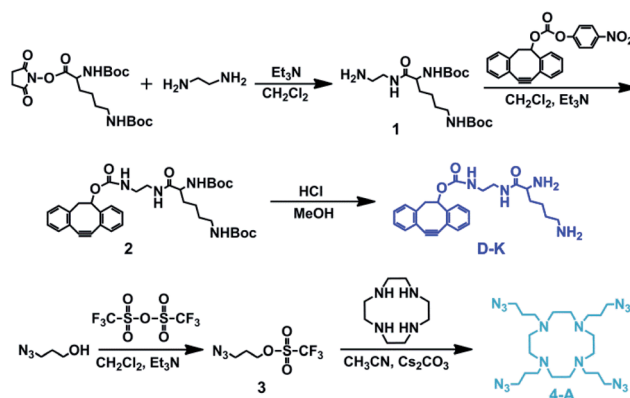

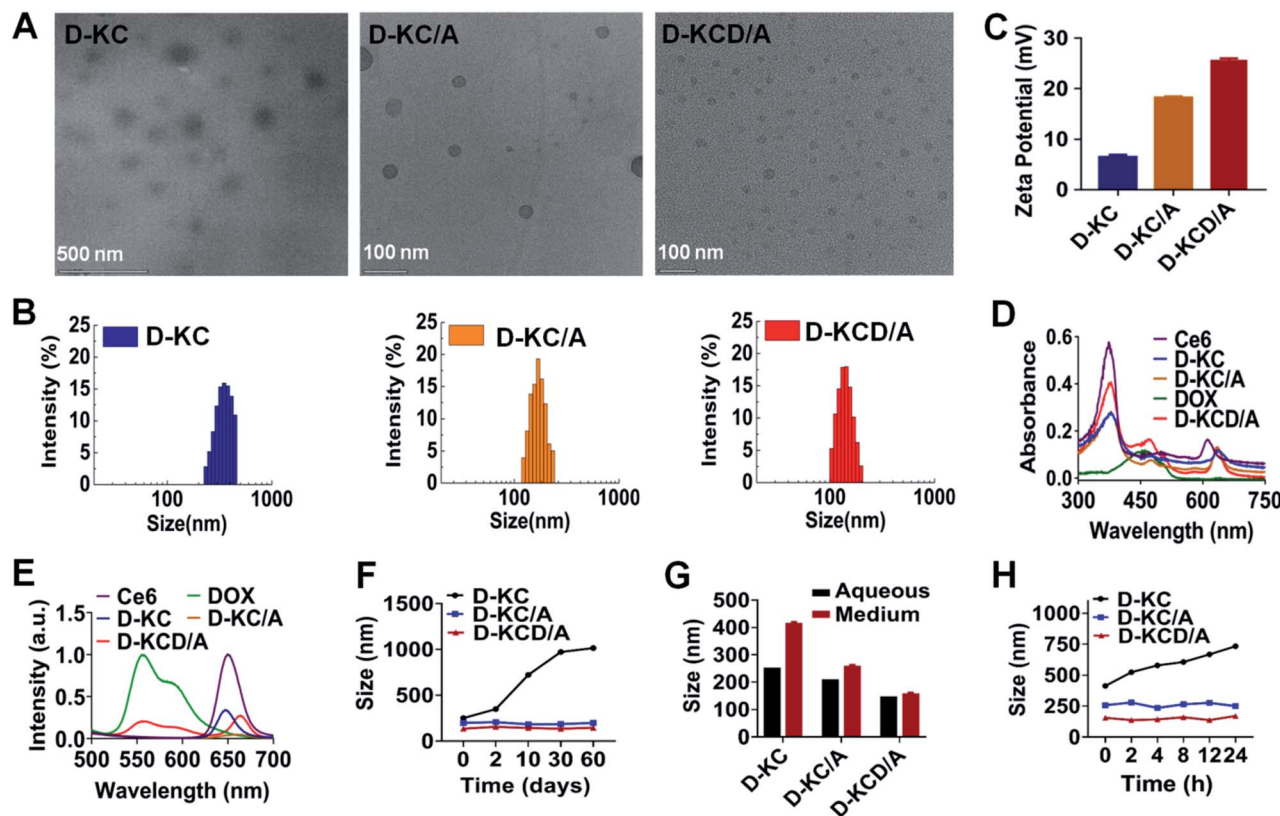
Fig. 1 The synthetic route to **D-K** and **4-A**.

Fig. 2 Characterization of various drug nanoparticles based on D-K mediated self-assembly. (A) TEM images, (B) size distributions, and (C) zeta potentials of different D-K regulated self-assembled nanoparticles. (D) UV-visible absorption and (E) fluorescence spectra of monomeric Ce6, monomeric DOX and various self-assembled nanoparticles. The excitation wavelength of Ce6 is 400 nm and that of DOX is 488 nm. (F) Long-term storage stability of various assembled nanoparticles in aqueous solution. The results indicated that assembled nanoparticles with cross-linking agents exhibited good stability in aqueous solution for at least two months. (G) Serum stability of the assembled nanoparticles after incubation with cell medium containing 10% (w/w) fetal bovine serum (FBS). The assembled nanoparticles showed a stable dispersion in the cell culture medium with minimal size increases due to the protein adsorption in the medium. (H) Size change of various assembled Ce6 nanoparticles over time in cell medium containing 10% (w/w) fetal bovine serum (FBS).

may be due to the fact that DLS provided the hydrodynamic diameter of nanoparticles with a hydride corona, while the TEM image depicted the real size of dry state samples. In addition, UV-vis absorption and fluorescence spectroscopy were applied to investigate the intermolecular interactions to gain insight into the molecular configuration and arrangement of the self-assembled nanostructures (Fig. 2D and E). In comparison to monomeric Ce6, D-KC showed a weak red-shifted absorbance in both the Soret and Q bands, due to Ce6 aggregation. The crosslinking of 4-A enhanced the Q-band absorption of Ce6 in D-KC nanoparticles, indicating the formation of a stable Ce6 complex. The integration of DOX into D-KC/A could enhance the absorption of Ce6. Moreover, we found that the fluorescence of D-KC and D-KC/A dramatically decreased due to the aggregation of assembled Ce6 ($\lambda_{ex} = 400$ nm), compared with monomeric Ce6. However, the fluorescence of Ce6 was partially restored after integrating DOX; meanwhile, the fluorescence of DOX ($\lambda_{ex} = 488$ nm) was greatly quenched. All these data indicate that D-K mediated self-assembly can effectively integrate Ce6 into nanoplatforms and DOX could coordinate with Ce6 and D-K to further increase the intermolecular hydrophobic and electrostatic interactions.[38] The loading efficiency of both Ce6

and DOX was 17%, respectively. Notably, the assembled D-KC/A and D-KCD/A nanoparticles with cross-linking agents were stable both in aqueous solution and culture medium (Fig. 2F–H), thus facilitating further biological applications.

Cellular uptake and nuclear accumulation of various self-assembled nanoparticles regulated by D-K

To investigate the capability of self-assembled nanoparticles to improve the cellular uptake and nuclear localization of Ce6 and DOX, breast cancer 4T1 cells were incubated with free Ce6, D-KC, D-KC/A or D-KCD/A for 2 h, followed by imaging with a fluorescence microscope. The cell nucleus was stained with 4,6-diamidino-2-phenylindole (DAPI) for identifying nuclear accumulation. As shown in Fig. 3A, all self-assembled nano-formulations were effectively transported into the cells, while free Ce6 exhibited weak intracellular uptake. Importantly, 4-A mediated click crosslinking in the nanoparticles facilitated nuclear translocation, causing a high accumulation of Ce6 and DOX in the nucleus (Fig. 3B and C). These data demonstrate that D-K coordinated self-assembly provides a potent strategy to improve cellular uptake and nuclear targeting of drugs.
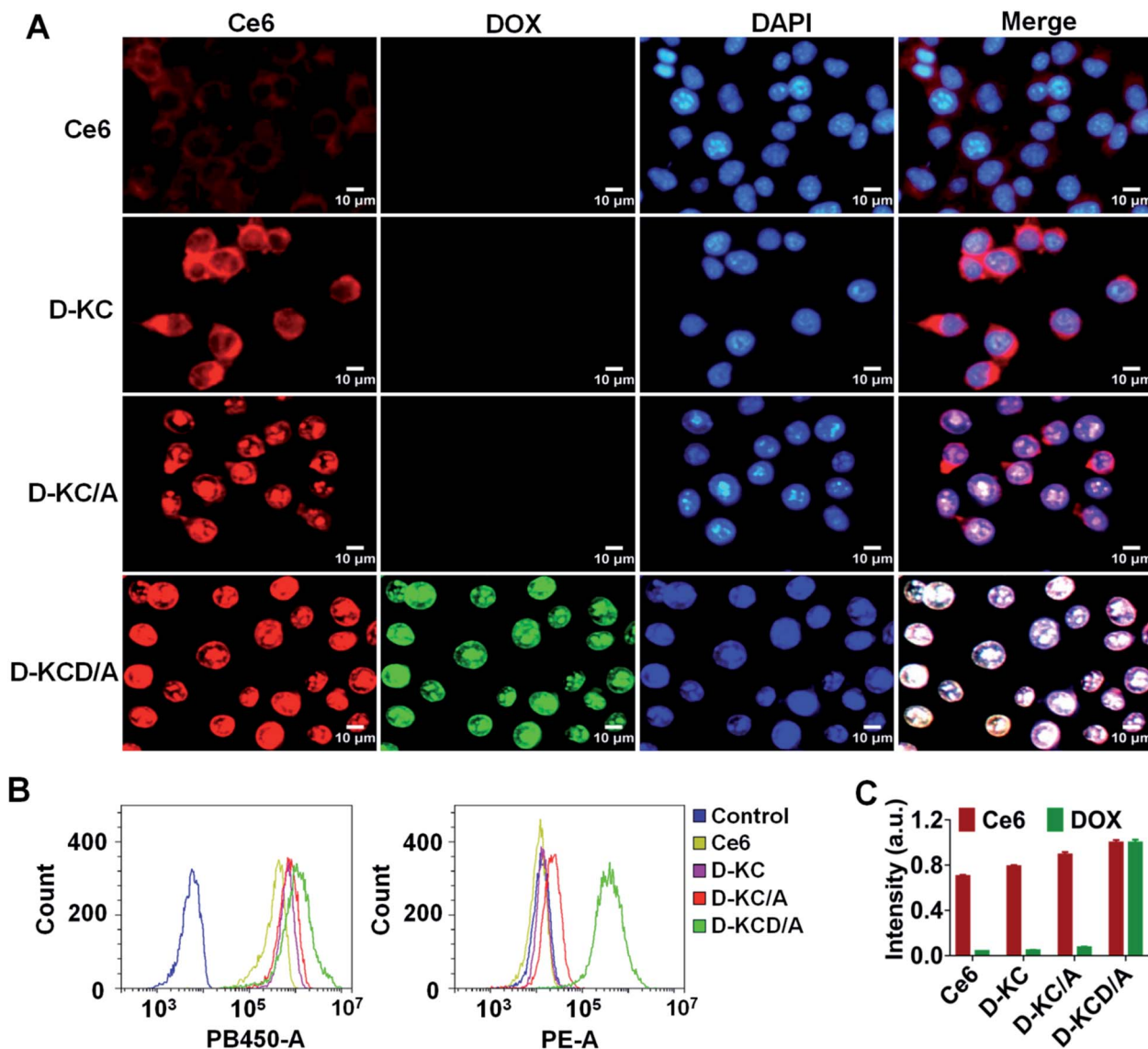
Fig. 3 Cellular uptake and nuclear accumulation of various self-assembled nanoparticles. (A) Fluorescence images of the intracellular location of free Ce6 and its various assembled nanoparticles after incubation with 4T1 cells. Scale bars: 10 μm. (B) Representative flow cytometry histograms and (C) quantitative analysis of the uptake of different self-assembled nanoparticles regulated by D-K (PB450: ex 405 nm, em 660 nm; PE: ex 488 nm, em 585 nm).

Cellular transport mechanism and *in vitro* antitumor efficacy

In consideration of the fact that endocytosis is a critical step in determining the intranuclear accumulation of nanoparticles, we evaluated the cellular uptake mechanism of D-KCD/A. As shown in Fig. 4A, compared with the control group, the cellular uptake of D-KCD/A nanoparticles was significantly reduced at 4 °C, or by pretreatment with sodium azide (an adenosine triphosphate consumptive agent). In addition, a low uptake of D-KCD/A was also observed in cells treated with genistein or methyl-β-cyclodextrin (M-β-CD), indicating that caveolin and lipid raft associated pathways are involved in the cellular internalization process. Taken together, these results suggest that D-KCD/A is actively transported in cells through multiple endocytic pathways, leading to enhanced cellular uptake. Next,

we also investigated the nuclear transportation mechanism of D-KCD/A. Cells were preincubated with ivermectin, a specific inhibitor of importin (ImP) mediated nuclear import, followed by incubating D-KCD/A. Minimal inhibition of the nuclear localization of D-KCD/A was observed (Fig. 4B), indicating that the intranuclear entry of D-KCD/A was ImP-independent.

To identify the therapeutic potential of D-KCD/A, the generation of singlet oxygen ($^1O_2$) under light irradiation (660 nm, 100 mW cm^{-2}, 2 min) was measured using singlet oxygen sensor green (SOSG). It was clear that D-KCD/A had no effects on the singlet oxygen production efficiency of Ce6 in NaCl solution (Fig. 4C). In addition, the fluorescence of Ce6 can be recovered in a high ionic strength environment (Fig. S1†), which further indicated the decomposition of nanoparticles and the release of Ce6, thus achieving effective PDT activation.
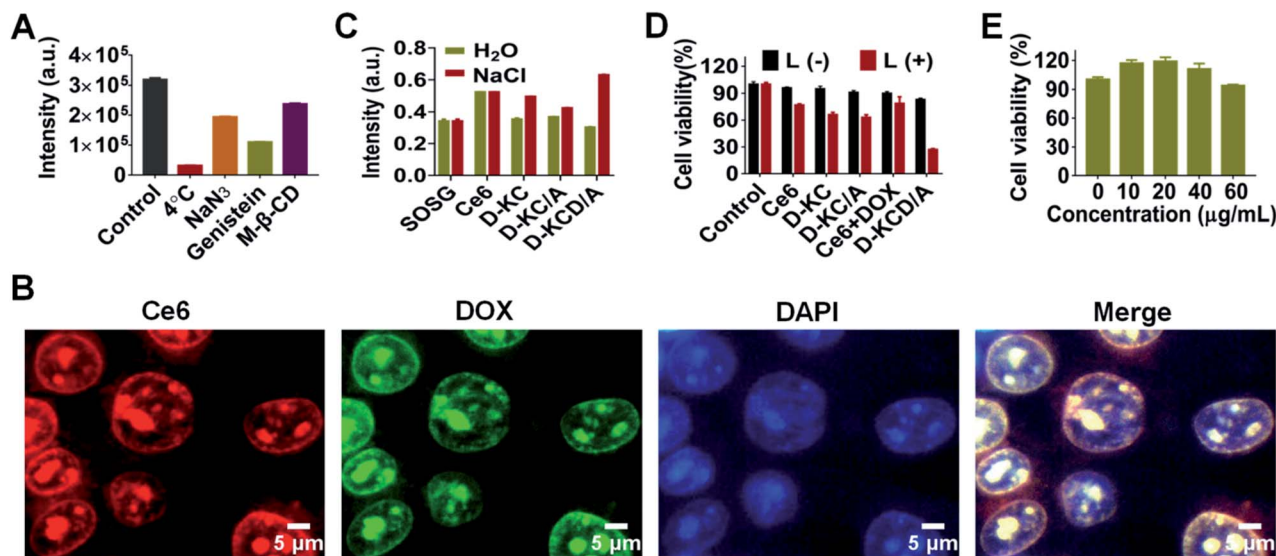
Fig. 4 Cellular transport mechanism and *in vitro* cytotoxicity. (A) Effects of various inhibitors (4 °C, NaN₃, M-β-CD and genistein) on cellular uptake of D-KCD/A nanoparticles. (B) Fluorescence images of the cellular location of D-KCD/A nanoparticles in the presence of an importin inhibitor (ivermectin). Scale bars: 5 μm. (C) The singlet oxygen generation capacity of different Ce6 nano-formulations determined by measuring the absorption intensity of SOSG under 660 nm LED light. (D) Cytotoxicity of free Ce6 and its various assembled nanoparticles with or without irradiation. (E) Relative viabilities of 4T1 cells after incubation with different concentrations of D-K.

Moreover, cell survival assay clearly revealed that the anticancer efficacy of both D-KC and D-KC/A was much higher than that of free Ce6 (Fig. 4D). Notably, D-KCD/A exhibited the highest cytotoxicity, confirming the synergistic effects of nucleus-targeted chemo-photodynamic therapy. Meanwhile, no apparent cytotoxicity was observed in any of the treatments without light stimulation (Fig. 4E), suggesting the good biocompatibility of **D-K**. These data indicate the great potential of self-assembled nanoformulations for cancer treatment.

Biodistribution

We next investigated the *in vivo* distribution of D-KCD/A in a 4T1 tumor xenograft mouse model. Free Ce6, D-KC/A, and D-KCD/A were intravenously injected into the mice and the fluorescence was imaged *in vivo* and *ex vivo*. Fig. 5A shows that both D-KC/A and D-KCD/A rapidly accumulated in tumor tissues, and generated strong fluorescent signals 8 h after injection. The strong fluorescence could even be observed for up to 24 h, indicating their tumor specificity. In contrast, mice treated with
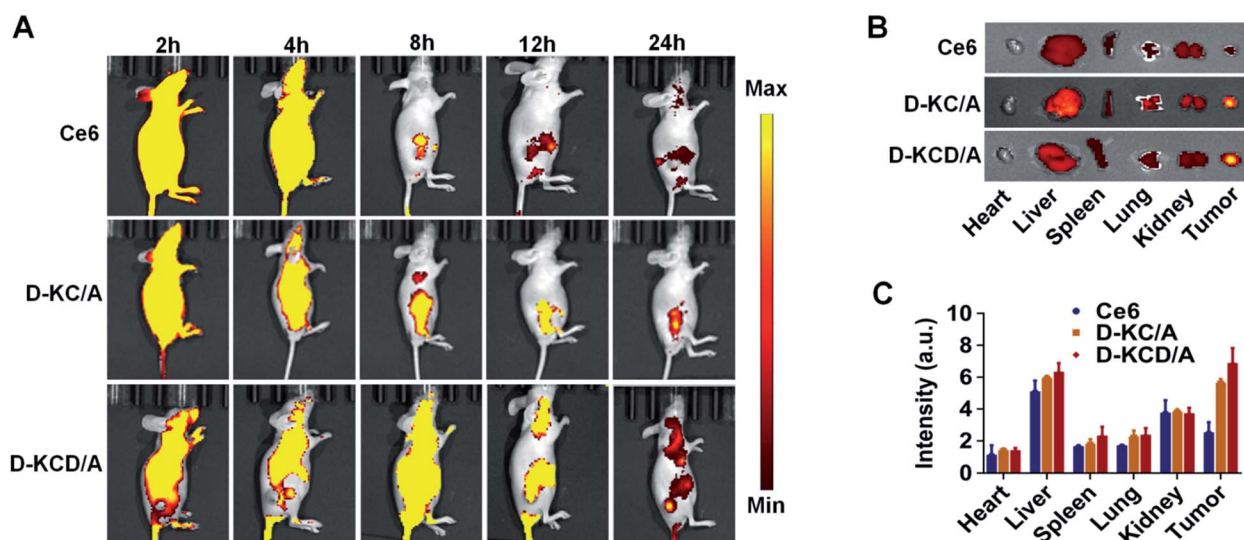

Fig. 5 *In vivo* biodistribution of different self-assembled Ce6 nanoparticles. (A) Whole body fluorescence images of 4T1 tumor-bearing nude mice at different time points after intravenous injection of free Ce6, D-KC/A and D-KCD/A nanoparticles. (B) *Ex vivo* fluorescence images and (C) quantification of fluorescence intensities of the tumors and major organs derived from the mice 24 h after injection.
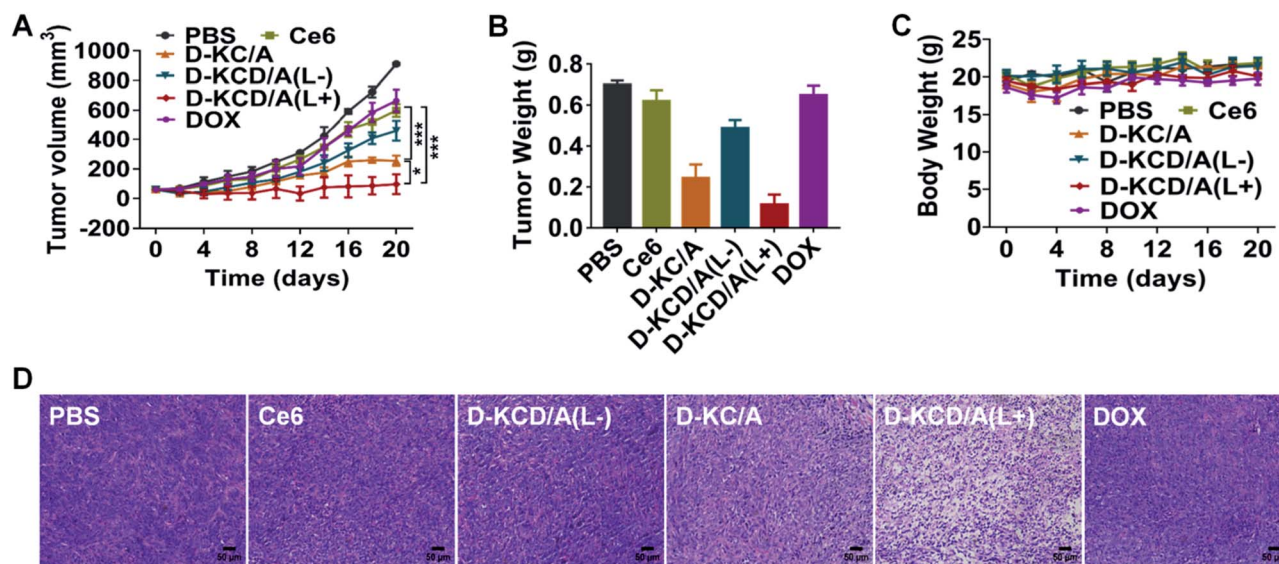
Fig. 6 *In vivo* antitumor effect. (A) Change in tumor volume of mice treated with free Ce6, DOX, D–KC/A and D–KCD/A nanoparticles with equivalent amounts of Ce6 (2 mg kg^{-1}) and DOX (2 mg kg^{-1}) followed by irradiation (660 nm, 200 mW cm^{-2}, 10 min). (B) Weight of the excised tumors after treatments. (C) Variation in the body weight of mice during different treatments. *$p < 0.05$, ***$p < 0.001$. Data are presented as mean $\pm$ SD ($n = 5$). (D) H&E staining of tumor tissues. Scale bars: 50 μm.

free Ce6 showed weak fluorescence at tumor sites, and the fluorescence greatly attenuated 24 h after injection, due to low tumor uptake and fast clearance of free Ce6. *Ex vivo* imaging of major organs and tumors harvested 24 h post injection further confirmed the enhanced tumor accumulation and retention of self-assembled Ce6 nanoparticles (Fig. 5B), which was also validated by the quantitative results obtained from the region-of-interest analyses (Fig. 5C).

In vivo antitumour activity

Based on the above results, we systematically evaluated the *in vivo* antitumor efficacy of self-assembled Ce6 nanoparticles in 4T1 tumor-bearing mice. As shown in Fig. 6A, tumor growth was effectively inhibited by Ce6 loaded D–KC/A nanoparticles under laser irradiation (660 nm, 200 mW cm^{-2}, 10 min), while minimal tumor inhibition was observed in mice treated with free Ce6. Importantly, Ce6 and DOX co-loaded D–KCD/A nanoparticles showed the best anticancer effects, suggesting enhanced anticancer effects of synergistic chemo-photodynamic therapy. Furthermore, tumor weights were measured at the end of the experiment, and demonstrated the optimal therapeutic effect of D–KCD/A nanoparticles (Fig. 6B), confirming the importance of combination therapy. Moreover, hematoxylin and eosin (H&E) staining revealed that self-assembled Ce6 nanoparticles including D–KC/A and D–KCD/A caused significant necrosis in the tumor tissue under light irradiation (Fig. 6D). In contrast, negligible damage was observed in healthy organs, such as the heart, liver, spleen, lungs, and kidneys (Fig. S2†). Meanwhile, minimal changes in body weights were observed during treatment (Fig. 6C), indicating their good biocompatibility. All these results suggest that the D–KCD/A multi-component nanoplatform is a promising strategy for cancer treatment.

Conclusions

In summary, we present a facile and robust multi-component amphiphilic amino acid based nanoplatform for enhancing simultaneous intranuclear delivery of PS and anticancer drugs. In this strategy, Ce6 and DOX were directly used as building blocks to construct well-defined nanoparticles through cyclo-octyne functionalized lysine (D-K) regulated self-assembly, which could avoid the utilization of any organic solvents or other tedious post-processing steps. The self-assembled nano-drugs showed enhanced cellular uptake and nuclear accumulation of Ce6 and DOX, and could not only significantly improve their cytotoxicity in cancer cells, but also minimize side effects. Importantly, D–KCD/A could selectively accumulate and retain in the tumor site, and exhibited optimal tumor growth inhibition *via* a multi-modal tumor suppressive effect induced by PDT and chemotherapy. Notably, the traditional amino acid protecting group Fmoc was changed to the DIBO functional group, and thus through changing the azide containing crosslinkers, a series of novel nucleus-targeting nanomaterials can be prepared simply and rapidly based on a copper-free click reaction with D-K, which can effectively expand the types of self-assembly material and enhance the self-assembly behavior under mild conditions. Therefore, our work proves the great potential of clickable amino acid derivatives as attractive and powerful tools for developing a self-assembled multi-component nucleus-targeted delivery nanoplatform for cancer treatment.

Ethical statement

All animal experiments were carried out in compliance with the requirements of the National Act on the Use of Experimental

Animals (People's Republic of China) and were approved by the Experimental Animal Ethical Committee of Chongqing University Cancer Hospital.

Author contributions

X. F. and X. N. conceived the project and designed the experiments. L. Y. and X. H. synthesized the chemicals. L. Y. and H. M. performed the cell experiments and analyzed the data. L. Y., Z. Z., J. T. and D. Q. performed the animal experiments. X. F., X. N., and H. C. supervised the project. All of the authors were involved in the analysis and interpretation of data. X. F., X. N., L. Y., X. H., and H. C. wrote the paper, with the help of the co-authors.

Conflicts of interest

The authors declare no conflicts of interest.

Acknowledgements

Notes and references

1 L. N. Abdullah and E. K.-H. Chow, *Clin. Transl. Med.*, 2013, **2**, 3.
2 C. Holohan, S. V. Schaeybroeck, D. B. Longley and P. G. Johnston, *Nat. Rev. Cancer*, 2013, **13**, 714–726.
3 C. He, K. Lu, D. Liu and W. Lin, *J. Am. Chem. Soc.*, 2014, **136**, 5181–5184.
4 T.-M. Sun, J.-Z. Du, Y.-D. Yao, C.-Q. Mao, S. Dou, S.-Y. Huang, P.-Z. Zhang, K. W. Leong, E.-W. Song and J. Wang, *ACS Nano*, 2011, **5**, 1483–1494.
5 J. Liu, L. Song, S. Liu, S. Zhao, Q. Jiang and B. Ding, *Angew. Chem., Int. Ed.*, 2018, **130**, 15486–15490.
6 D.-W. Zheng, J.-L. Chen, J.-Y. Zhu, L. Rong, B. Li, Q. Lei, J.-X. Fan, M. Z. Zou, C. Li, S.-X. Cheng, *et al.*, *Nano Lett.*, 2016, **16**, 4341–4347.
7 L. Wang, Q. Sun, X. Wang, T. Wen, J.-J. Yin, P. Wang, R. Bai, X.-Q. Zhang, L.-H. Zhang, A.-H. Lu and C. Chen, *J. Am. Chem. Soc.*, 2015, **137**, 1947–1955.
8 H. Lee, J. Han, H. Shin, H. Han, K. Na and H. Kim, *J. Control Release*, 2018, **283**, 190–199.
9 T. Wang, D. Wang, J. Liu, B. Feng, F. Zhou, H. Zhang, L. Zhou, Q. Yin, Z. Zhang, Z. Cao, H. Yu and Y. Li, *Nano Lett.*, 2017, **17**, 5429–5436.
10 W. Chen, J. Liu, Y. Wang, C. Jiang, B. Yu, Z. Sun and L. Lu, *Angew. Chem., Int. Ed.*, 2019, **58**, 6290–6294.
11 Y.-X. Zhu, H.-R. Jia, G.-Y. Pan, N. W. Ulrich, Z. Chen and F.-G. Wu, *J. Am. Chem. Soc.*, 2018, **140**, 4062–4070.
12 L. Wu, X. Cai, H. Zhu, J. Li, D. Shi, D. Su, D. Yue and Z. Gu, *Adv. Funct. Mater.*, 2018, **28**, 1804324.
13 J. F. Lovell, T. W. B. Liu, J. Chen and G. Zheng, *Chem. Rev.*, 2010, **110**, 2839–2857.
14 D. Liu, B. Chen, Y. Mo, Z. Wang, T. Qi, Q. Zhang and Y. Wang, *Nano Lett.*, 2019, **19**, 6964–6976.
15 S. Yan, X. Zeng, Y. Tang, B.-F. Liu, Y. Wang and X. Liu, *Adv. Mater.*, 2019, **31**, 1905825.
16 W. Sun, L. Luo, Y. Feng, Y. Cai, Y. Zhuang, R. Xie, X. Chen and H. Chen, *Angew. Chem., Int. Ed.*, 2020, **59**, 9914–9921.
17 C. Xu, J. Nam, H. Hong, Y. Xu and J. J. Moon, *ACS Nano*, 2019, **13**, 12148–12161.
18 G. Pasparakis, T. Manouras, M. Vamvakaki and P. Argitis, *Nat. Commun.*, 2014, **5**, 3623.
19 Y. Li, T.-Y. Lin, Y. Luo, Q. Liu, W. Xiao, W. Guo, D. Lac, H. Zhang, C. Feng, S. Wachsmann-Hogiu, *et al.*, *Nat. Commun.*, 2014, **5**, 4712.
20 S. H. Lim, C. Thivierge, P. Nowak-Sliwinska, J. Han, H. Van Den Bergh, G. Wagnières, K. Burgess and H. B. Lee, *J. Med. Chem.*, 2010, **53**, 2865–2874.
21 T. Aida, E. W. Meijer and S. I. Stupp, *Science*, 2012, **335**, 813–817.
22 B. H. Northrop, Y.-R. Zheng, K.-W. Chi and P. J. Stang, *Acc. Chem. Res.*, 2009, **42**, 1554–1563.
23 C. Rest, R. Kandanelli and G. Fernandez, *Chem. Soc. Rev.*, 2015, **44**, 2543–2572.
24 B. O. Okesola and A. Mata, *Chem. Soc. Rev.*, 2018, **47**, 3721–3736.
25 D. M. Raymond and B. L. Nilsson, *Chem. Soc. Rev.*, 2018, **47**, 3659–3720.
26 X. Zhang, Z.-K. Chen and K. P. Loh, *J. Am. Chem. Soc.*, 2009, **131**, 7210–7211.
27 R. Zou, Q. Wang, J. Wu, J. Wu, C. Schmuck and H. Tian, *Chem. Soc. Rev.*, 2015, **44**, 5200–5219.
28 J. Wang, K. Liu, R. Xing and X. Yan, *Chem. Soc. Rev.*, 2016, **45**, 5589–5604.
29 K. Tao, A. Levin, L. Adler-Abramovich and E. Gazit, *Chem. Soc. Rev.*, 2016, **45**, 3935–3953.
30 Q. Zou and X. Yan, *Chemistry*, 2018, **24**, 755–761.
31 M. Kumar, N. L. Ing, V. Narang, N. K. Wijerathne, A. I. Hochbaum and R. V. Ulijn, *Nat. Chem.*, 2018, **10**, 696–703.
32 Y. Li, Q. Zou, C. Yuan, S. Li, R. Xing and X. Yan, *Angew. Chem., Int. Ed.*, 2018, **57**, 17084–17088.
33 S. Bera, B. Xue, P. Rehak, G. Jacoby, W. Ji, L. J. W. Shimon, R. Beck, P. Král, Y. Cao and E. Gazit, *ACS Nano*, 2020, **14**, 1694–1706.
34 P. Xing, S. Z. F. Phua, X. Wei and Y. Zhao, *Adv. Mater.*, 2018, **30**, 1805175.
35 H. Cao, Q. Yuan, X. Zhu, Y.-P. Zhao and M. Liu, *Langmuir*, 2012, **28**, 15410–15417.
36 K. Liu, R. Xing, Q. Zou, G. Ma, H. Möhwald and X. Yan, *Angew. Chem., Int. Ed.*, 2016, **55**, 3036–3039.
37 H. Zhang, K. Liu, S. Li, X. Xin, S. Yuan, G. Ma and X. Yan, *ACS Nano*, 2018, **12**, 8266–8276.
38 S. Li, Q. Zou, Y. Li, C. Yuan, R. Xing and X. Yan, *J. Am. Chem. Soc.*, 2018, **140**, 10794–10802.